Measurement 127 (2018) 68–77

Contents lists available at ScienceDirect

Measurement

journal homepage: www.elsevier.com/locate/measurement

A time domain reconstruction method of randomly sampled frequency sparse signal

Imrich Andráš*, Pavol Dolinský, Linus Michaeli, Ján Šaliga

Department of Electronics and Multimedia Communications, Faculty of Electrical Engineering and Informatics, Technical University of Košice, Letná 9, 042 00 Košice, Slovak Republic

ARTICLE INFO

Keywords:
Sparse signal
Analog-to-information conversion
Compressed sensing
Nonuniform sampling
Stochastic sampling

ABSTRACT

In this paper stochastic sampling as a method of frequency sparse signal acquisition is presented. Basic principle of compressed sensing is reviewed, with emphasis on nonuniform sampling and signal reconstruction methods. A robust time domain reconstruction method of randomly sampled signal through compressed sensing approach is proposed. The presented reconstruction algorithm is evaluated by means of simulations, with comparison to conventional compressed sensing reconstruction and the most common practical issues taken into account. Simulation results indicate that the proposed reconstruction method is resistent to high levels of quantization and uncorrelated noise. Experiments with real hardware were also performed, results of which confirm the ability of stochastic sampling framework to overcome the Nyquist limit of analog-to-digital converters.

1. Introduction

In recent years, compressive sensing (CS) came up as a promising method of sub-Nyquist sampling. It is a powerful tool for signal analysis, and it allows to acquire signals with fewer measurements then previously thought possible. This is accomplished by exploiting the fact that many real-world signals have far fewer degrees of freedom than the signal size might indicate. For instance, spectrally sparse (narrowband) signal depends upon only a few degrees of freedom, although its total bandwidth is exceptionally wide. Nyquist sampling of such signal is difficult, and it requires the storage of significantly large amounts of data. With sparse signals, CS allows for much lower sampling frequencies. The result is lower output data transfer rate, and there is a possibility of overcoming the speed limit of conventional analog-to-digital converters (ADCs). Lower sampling rate by extension also means reduction of power consumption, and lower demands on communication channels. A wide field of possible applications could benefit from these advantages, e. g. wireless sensor networks.

Two most promising methods of CS have been proposed and are discussed in literature, random modulation pre-integration (RMPI), and nonuniform sampling. This work is focused on nonuniform sampling, or more specifically, the stochastic sampling (SS) architecture ([1,2]). This architecture has to be distinguished from adaptive ADCs [3,4] that also perform nonuniform sampling.

RMPI architectures have been extensively studied and successfully used ([5,6]), but they are difficult to implement. Before the signal can be sampled with a lower rate, it has to be conditioned by specialized analog circuitry operating at Nyquist rates [8]. The precise nonideal nature of this circuitry, such as the modulation signal shape [9], jitter [10] and the filter impulse response [11] need to be precisely modelled in order to ensure low reconstruction error. SS is very promising in this regard, because there is no circuitry required besides the ADC. Peak sampling frequency of this ADC may be lower than the Nyquist rate, and the signal can be reconstructed assuming its frequency band is known. Certain applications could also benefit from the fact that the SS framework is inherently resistant to data loss [12].

The implementation of random sampler and the reconstruction algorithm will be discussed, from which the latter is not extensively covered by literature. Evaluation of the proposed algorithm is presented, with regards to practical issues such as inherent and quantization noise.

2. The principle of compressed sensing

The main goal of CS is transforming a signal to a suitable descriptive domain and condensing it into a few samples, which is referred to as analog-to-information conversion (AIC). This compressed information is then sent to the receiver, where the original signal is reconstructed. No information loss and exact reconstruction is theoretically possible with CS, with high potential compression ratios.

In order for CS to be applicable, it is assumed that the input signal can be represented by a linear combination of known basis functions.

* Corresponding author.
E-mail addresses: imrich.andras@tuke.sk (I. Andráš), pavol.dolinsky@tuke.sk (P. Dolinský), linus.michaeli@tuke.sk (L. Michaeli), jan.saliga@tuke.sk (J. Šaliga).

https://doi.org/10.1016/j.measurement.2018.05.065
Received 13 December 2016; Received in revised form 16 February 2018; Accepted 17 May 2018
Available online 26 May 2018
0263-2241/

Furthermore, the signal must be *sparse*, meaning that it consists of only a small number of basis functions. The signal composed of s basis functions is denoted to be s-sparse. Let us define L basis vectors $\boldsymbol{\psi}_l \in \mathbb{R}^{N\times 1}$, $1 \leqslant l \leqslant L$ to represent any possible input signal components. The columns of the basis matrix $\boldsymbol{\Psi} \in \mathbb{R}^{N\times L}$ consist of these basis vectors. The input signal vector $\mathbf{f} \in \mathbb{R}^{N\times 1}$ can then be described as

$$\mathbf{f} = \boldsymbol{\Psi}\mathbf{x} \tag{1}$$

where the s-sparse vector $\mathbf{x} \in \mathbb{R}^{L\times 1}$ conducts the linear combination [13].

2.1. Analog-to-information conversion

Conventional ADCs acquire signal samples at equidistant time instants, according to the Nyquist sampling theorem. With signals highly sparse at a certain domain, such sampling means great redundancy in acquired data, since the amount of information contained within a sparse signal is limited. AIC exploits this fact, and only takes a limited number of samples, sufficient to represent the information content. High bandwidth sparse signals can be precisely measured by time-equivalent sampling as well, and reconstructed by a very simple algorithm [14]. This approach however relies on the signal being stationary for a prolonged time period. CS employs different sampling and reconstruction strategies and in general does not require the measured signal to be stationary.

The input signal $\mathbf{f} \in \mathbb{R}^{N\times 1}$ is correlated with $M < N$ measurement signals, represented by M rows of the measurement matrix $\boldsymbol{\Phi} \in \mathbb{R}^{M\times N}$. This performs the AIC, with resulting information signal vector

$$\mathbf{y} = \boldsymbol{\Phi}\mathbf{f} \in \mathbb{R}^{M\times 1} \tag{2}$$

Let the input signal vector be s-sparse on basis $\boldsymbol{\Psi}$, and let bases $\boldsymbol{\Psi}$ and $\boldsymbol{\Phi}$ be incoherent (rows $\boldsymbol{\varphi}_m$ of $\boldsymbol{\Phi}$ do not sparsely represent the columns $\boldsymbol{\psi}_l$ of $\boldsymbol{\Psi}$, and vice versa). If $s < M \ll N$, input signal can be reconstructed [15]. According to [13], an approximation of minimal M needed is given by

$$M_{\min} = \mu s \log_{10}(N) \tag{3}$$

assuming zero or negligible noise [16]. $\mu = 1$ for incoherent bases, but has to be increased to $\mu = L/N$ if $N < L$. By inserting (1) into (2) the information signal becomes

$$\mathbf{y} = \boldsymbol{\Phi}\boldsymbol{\Psi}\mathbf{x} \tag{4}$$

with the reconstruction matrix

$$\mathbf{A} = \boldsymbol{\Phi}\boldsymbol{\Psi} \in \mathbb{R}^{M\times L}. \tag{5}$$

2.2. Reconstruction

At the receiving end of CS framework, the information signal $\mathbf{y}$, and both bases $\boldsymbol{\Psi}$ and $\boldsymbol{\Phi}$ are known. The only unknown required for reconstruction of (1) is $\mathbf{x}$. If $\mathbf{A}$ was a square matrix (which would mean applying conventional Nyquist sampling), the problem could be solved simply by inverting $\mathbf{A}$. But since $\mathbf{A}$ is a rectangular matrix, it cannot be simply inverted, and an undetermined system of M equations and L unknowns is to be solved. Here the importance of sparsity turns out, because based on this requirement a unique solution can be found. Out of all the possible solutions, the right solution is the one that is the most sparse [17].

The sparsity s of vector $\mathbf{x}$ is in general its ℓ_0 pseudo-norm, defined as the number of non-zero elements:

$$\ell_0 = \|\mathbf{x}\|_0 := \{i: x_i \neq 0\} \tag{6}$$

Sparsity is an additional information, used to construct the measurement matrix $\boldsymbol{\Phi}$, and forming an optimization problem

$$\min\|\mathbf{x}\|_0 \text{ subject to } \mathbf{A}\mathbf{x} = \mathbf{y} \tag{7}$$

Based on the ideal definition of sparsity (6), it should be trivial to find s simply by performing the AIC and counting the number of non-zero elements of $\mathbf{y}$. However, for any real signal with inherent noise, there are a few elements of large value, and other elements small but not zero [18]. To address this issue, other metrics were proposed [19]. In [20] it was deduced, that with highly sparse signals the norm

$$\ell_1: \|\mathbf{x}\|_1 = \sum_{i=1}^{n} |x_i| \tag{8}$$

can be used, which is preferable since it leads to a convex optimization problem

$$\min\|\mathbf{x}\|_1 \text{ subject to } \mathbf{A}\mathbf{x} = \mathbf{y} \tag{9}$$

This guarantees a correct optimal solution, if such exists. Moreover, efficient algorithms may be used – with the highly unstable ℓ_0 norm, only brute force methods are successful. With complying to (9) the original signal estimate can be found as

$$\hat{\mathbf{f}} = \boldsymbol{\Psi}(\mathbf{A}^T\mathbf{A})^{-1}\mathbf{A}^T\mathbf{y} \tag{10}$$

where $(*)^{-1}$ denotes the pseudoinverse matrix of $*$.

Another issue with CS is determining the base matrices $\boldsymbol{\Psi}$ and $\boldsymbol{\Phi}$. For some signals, their sparse domain is known, e. g. frequency or wavelet. For other there is not a specific domain for this purpose, and a suitable dictionary must be learned. Correctly constructed set $\boldsymbol{\Psi}$ of basic functions ensures high compression ratio and low reconstruction error.

As for the measurement matrix $\boldsymbol{\Phi}$, pseudo-random elements are used to ensure the incoherence of bases. With CS architectures such as RMPI ([5–7,9–11]), measurement matrix consists of randomly placed ± 1's and it must be full-rank. The *SS* architecture simply takes samples of the input signal at random time instants. For the implementation of SS, only a vector containing random sequence of 0's and 1's is needed. To be consistent with mathematical descriptions above, measurement matrix of SS would be a full-rank matrix of 0's, with a 1 placed in each row. Positions of 1's are random, but their column indices must be ascending. CS framework with both sensing and decoding side is summarized in Fig. 1.

3. Stochastic sampling

In order to subsample the Nyquist grid, SS exploits the incoherence of time and frequency. Subsampling is random – time instants at which the signal is sampled are selected randomly. Thus there is no coherent aliasing effect, meaning no frequency information loss, and the original signal can be recovered via nonlinear processing [1,2]. A conceptual diagram of SS is shown in Fig. 2.

SS takes Nyquist-rate samples of input signal and randomly discards most of the samples according to pseudo-random bit sequence (PRBS). Sampling is therefore random, but samples are spaced with integer multiples of underlying Nyquist rate. Additional digital signal processing (DSP) is applied in order to encode both sample values and their positions into the output data stream. Reduced power consumption and higher input bandwidth of SS may be achieved by using ADC triggered by PRBS, rather than discarding samples of a conventional ADC.

Let $F[\omega]$, $\omega = 2\pi\nu$ be the discrete Fourier transform (DFT) of

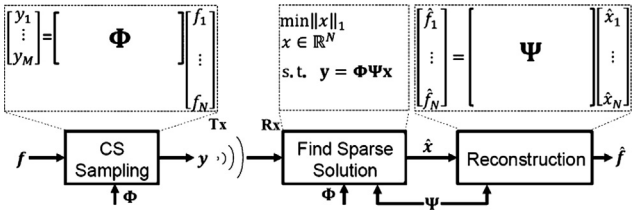

Fig. 1. Compressed sensing framework.

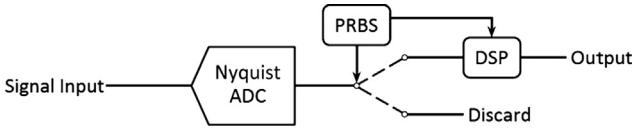

Fig. 2. Stochastic sampler.

uniformly sampled input signal f_n, $n = 1, 2, ...,N$. If the input signal is s-sparse in frequency domain, $F[\omega]$ has only s non-zero entries. Now only a subset Ξ of all the input samples is collected, with M sample locations chosen at random. According to [21], it is possible to exactly recover the input signal by solving

$$\min\|\hat{F}[\omega]\|_1 \text{ subject to } \forall\, \xi \in \Xi,\ \hat{f}_\xi = f_\xi \tag{11}$$

where $\hat{f}_\xi$ denotes the reconstructed signal. The minimization problem (11), however, assumes ideal sparse signal. In a practical application, inherent and quantization noise have to be considered, as well as nonideal sparsity discussed in Section 2.2. This calls for reformulation of (11):

$$\min\|\hat{F}[\omega]\|_1 \text{ subject to } \forall\, \xi \in \Xi,\ (\hat{f}_\xi - f_\xi) \leqslant \varepsilon \tag{12}$$

with the threshold ε to account for joint noise amplitude. It can be inferred that such a reconstruction cannot be exact, but the reconstructed signal agrees with the original up to the noise level.

Other Fourier domain reconstruction methods were also proposed. High precision of parameter estimation can be achieved by performing nonparametric interpolated DFT estimation of frequency [22]. Other parameters can then be found by iterative sine fit algorithm. Such an approach is not suitable for compressed sensing applications, since it estimates the parameters of only one sine component. The proposed implementation of the CS framework based on SS with differential evolution parameter estimation (DEPE) will now be introduced.

3.1. Implementation of the stochastic sampler

It is assumed, that the input signal $\mathbf{f} \in \mathbb{R}^{N\times 1}$ is a narrowband frequency-sparse signal that can be described as

$$f_n = \sum_{i=1}^{K} {}^{K}C_i \sin(2\pi\, {}^{K}\nu_i n T_s + {}^{K}\theta_i) + q_n,\ \ n = 1, 2, ...,N \tag{13}$$

Individual signal components are characterized by parameter vectors ${}^{K}\mathbf{C}$, ${}^{K}\boldsymbol{\nu}$, ${}^{K}\boldsymbol{\theta} \in \mathbb{R}^{K\times 1}$ defining their amplitudes, frequencies and phases respectively. Additive sources of noise are represented by q_n and T_s is the sampling period.

From all the samples of input signal (13), a subset of M samples is selected. Ξ contains indices of selected samples

$$\Xi = \{\xi_1, \xi_2, ...,\xi_M\} \tag{14}$$

Entries of Ξ are random numbers, following the rules

$$\forall\, m \in \mathbb{N},\ \ 1 \leqslant m \leqslant M\text{: } \xi_m \in \mathbb{N},\ \ 1 \leqslant \xi_m \leqslant N \tag{15}$$

$$\forall\, i, j \in \mathbb{N},\ \ 1 \leqslant i < j \leqslant M\text{: } \xi_i < \xi_j \tag{16}$$

Using (14), the elements of measurement matrix $\boldsymbol{\Phi}$ are obtained as

$$\phi_{i,j} = \begin{cases} 1\text{: } (i = m) \wedge (j = \xi_m), & m = 1, 2,...,M \\ 0 \end{cases} \tag{17}$$

and the information signal vector $\mathbf{y}$ (2) becomes:

$$y_m = f_{\xi_m},\ m = 1, 2, ...,M \tag{18}$$

Vector $\mathbf{y}$ (17) along with original sample positions Ξ (14) is passed to the reconstruction algorithm. Length M of $\mathbf{y}$ is chosen with respect to (3), based on expected signal sparsity.

3.2. Proposed reconstruction algorithm

In Section 3 the original minimization problem (11) from [21] was reformulated to make it less abstract. However, (12) is still somewhat impractical to implement. It requires the search for solutions that satisfy the condition $\forall\, \xi \in \Xi,\ (\hat{f}_\xi - f_\xi) \leqslant \varepsilon$, and choosing the solution that is the most sparse in Fourier domain.

Transition from (11), (12) causes great increase of the number of possible solutions. In order to find the right solution, the noise tolerance ε must be set as low as possible, but greater than the actual noise level. Choosing a suitable value of ε would be difficult in practice, since the actual noise level is usually not known and non-stationary. Moreover, (11) and (12) suggest reconstructing the input signal directly in frequency domain. This would require a large number of coefficients to be optimized, since Fourier transform of a signal has the same size as the signal itself. Another disadvantage is that frequency estimation in Fourier domain is bound to discrete frequency bins. This may be a problem in applications where high frequency resolution is required.

To overcome these issues, the following time domain DEPE algorithm is proposed. At first a scenario is considered, where the input signal (13) is composed of a known number of sinusoidal components k. The corresponding parameter vector estimates ${}^{k}\hat{\mathbf{C}}$, ${}^{k}\hat{\boldsymbol{\nu}}$, ${}^{k}\hat{\boldsymbol{\theta}} \in \mathbb{R}^{k\times 1}$ can be found by solving the problem

$$\{{}^{k}\hat{\mathbf{C}},\ {}^{k}\hat{\boldsymbol{\nu}},\ {}^{k}\hat{\boldsymbol{\theta}}\} = \arg\min_{{}^{k}\hat{\mathbf{C}},{}^{k}\hat{\boldsymbol{\nu}},{}^{k}\hat{\boldsymbol{\theta}}} \|\hat{\mathbf{y}} - \mathbf{y}\|_2 \tag{19}$$

$\mathbf{y}$ is the information signal vector obtained by sampling (18) of the input signal (13). The information signal vector estimate $\hat{\mathbf{y}}$ is given by the parameter vector estimates ${}^{k}\hat{\mathbf{C}}$, ${}^{k}\hat{\boldsymbol{\nu}}$, ${}^{k}\hat{\boldsymbol{\theta}}$, from (13) and (18) as

$$\hat{y}_m = \sum_{i=1}^{k} {}^{k}\hat{C}_i \sin(2\pi\, {}^{k}\hat{\nu}_i \xi_m T_s + {}^{k}\hat{\theta}_i),\ \ m = 1, 2, ...,M \tag{20}$$

In a practical application, the input signal is not ideally sparse, and thus the actual number of its components K is not known. However we assume, that a minimum and maximum number of components $k_{\min}, k_{\max} \in \mathbb{N}$ sufficient for successful reconstruction can be chosen.

Since the actual K is unknown, we propose to look for solutions of (19) for each $k = k_{\min}, k_{\min} + 1, ...,k_{\max}-1, k_{\max}$ and then choose the best one. With highly sparse narrowband signals containing only a few components, $k_{\max}-k_{\min}$ is a small number. Moreover, (19) is an optimization problem with stable ℓ_2 norm. Only a small number of coefficients is to be optimized by (19) for each k, which makes this approach numerically feasible.

In compressed sensing theory, reconstruction is led by minimizing the unstable ℓ_0 or ℓ_1 norm in order to obtain the most sparse solution. The aim was to eliminate the need to include such norms in optimization problems. To choose the optimal sparse solution, the objective errors

$${}^{k}O_F = \min_{{}^{k}\hat{\mathbf{C}},{}^{k}\hat{\boldsymbol{\nu}},{}^{k}\hat{\boldsymbol{\theta}}} \|\hat{\mathbf{y}} - \mathbf{y}\|_2 \tag{21}$$

and parameter vectors ${}^{k}\hat{\mathbf{C}}$, ${}^{k}\hat{\boldsymbol{\nu}}$, ${}^{k}\hat{\boldsymbol{\theta}}$ (18) are collected for each $k = k_{\min}, k_{\min} + 1, ...,k_{\max}-1, k_{\max}$. Sparsity of the frequency vector ${}^{k}\hat{\boldsymbol{\nu}}$ is then evaluated in order to penalize solutions with greater number of components. Number of reconstructed signal components $\hat{K}$ is chosen as

$$\hat{K} = \underset{k}{\operatorname{argmin}}({}^{k}O_F \| {}^{k}\hat{\boldsymbol{\nu}}\|_2) \tag{22}$$

Such a penalization is needed for cases when actual number of components is smaller than k. The optimization algorithm may still be yielding small error (21), but there are artificial components in the parameter vectors. This may cause noisy or distorted reconstructed signal. Distortions do not necessarily occur, but incorrect parameter vectors do. For example, one sine component may be split into more components with the same frequency and different amplitudes or

phases. Penalization (22) efficiently eliminates such cases, as its behavior emulates the originally proposed ℓ_0 norm in (7).

The proposed penalization (22) works well with noisy narrowband signals, however it is not optimal for all scenarios. Let the signal contain several components with large amplitudes and frequencies close together plus an additional component with small amplitude and substantially higher frequency. In such scenario, there will be only a small difference in ${}^{k}O_F$ with or without this stand-alone high frequency component. Penalization (22) will treat such a component as noise and discard it. Application specific modifications to (22) could be made in order to address this issue, e. g. using a different norm or evaluating ${}^{k}\hat{\mathbf{C}}$ instead of ${}^{k}\hat{\boldsymbol{\nu}}$.

With the parameter vectors known, the original signal $\hat{\mathbf{f}}$ can be reconstructed as

$$\hat{f}_n = \sum_{i=1}^{\hat{K}} {}^{\hat{K}}\hat{C}_i \sin(2\pi\, {}^{\hat{K}}\hat{\nu}_i n T_s + {}^{\hat{K}}\hat{\theta}_i), \quad n = 1, 2, \ldots, N \tag{23}$$

The computing efficiency greatly depends on the algorithm used to solve the optimization problem (19). Signal model (20) and the resulting objective function (21) are linear in amplitude ${}^{k}\hat{\mathbf{C}}$, but nonlinear in phase ${}^{k}\hat{\boldsymbol{\theta}}$ and frequency ${}^{k}\hat{\boldsymbol{\nu}}$. The contribution of phase to the objective function ${}^{k}O_F$ is nonlinear and periodic, but it remains almost unchanged by random sampling. Requirements on the optimization algorithm are defined mainly by the contribution of frequency. Even with Nyquist sampling, the frequency contribution to ${}^{k}O_F$ is a sinc-like function, which precludes the use of gradient based methods on a wide solution space. Furthermore, due to random sampling the original sinc-like function is deformed with pronounced local minima appearing, as is shown in an example in Fig. 3. The solving of (19) calls for a metaheuristic approach, as no assumptions about the optimization problem can be made other than the existence of a global optimum guaranteed by (3).

Differential evolution (DE) [23] was chosen for solving (19), since it can search large spaces of candidate solutions and find the global optimum with no regard of the parameters linearity. Due to the stochastic nature of candidate solution, there is no guarantee that the global optimum is found. In order for the reconstruction to be successful, large enough population size with enough iterations for improving the candidate solution must be used. The DE optimization process may become computationally unfeasible or contrary unreliable, which can be prevented by suitably set boundaries for amplitudes, frequencies, phases and the number of signal components. Let us denote the amplitude boundaries

$$C_{\min} \leqslant {}^{k}C_i \leqslant C_{\max} \tag{24}$$

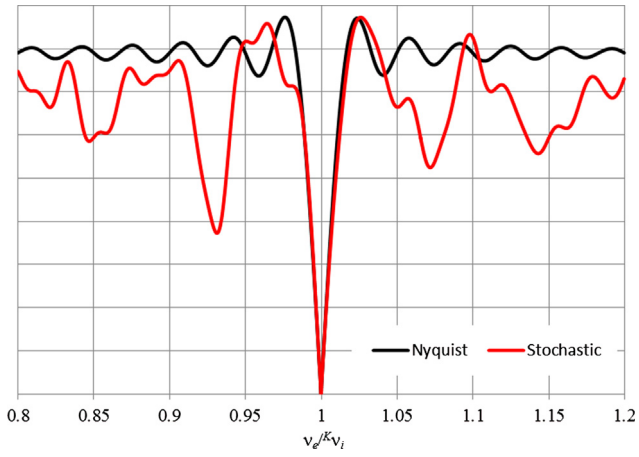

Fig. 3. Objective error vs. estimated frequency ν_e with Nyquist and stochastic sampling.

the phase boundaries

$$\theta_{\min} \leqslant {}^{k}\theta_i \leqslant \theta_{\max} \tag{25}$$

and the frequency boundaries

$$\nu_{\min} \leqslant {}^{k}\nu_i \leqslant \nu_{\max} \tag{26}$$

The proposed reconstruction algorithm is not sensitive to amplitude constraints (24). The constraints of phase (25) must not induce periodic minima, which is accomplished by setting $C_{\min} = -C_{\max}$, $\theta_{\min} = 0$ and $\theta_{\max} = \pi$. In the simulation and experimental results presented below it will be shown that the frequency interval (26) does not have to be particularly narrow, but the probability of successful reconstruction (PSR) can be improved by setting (26) as narrow as possible. In order to do this, a priori knowledge of the signal frequency band is needed. With no such knowledge, an initial approximation of the signal parameters could be obtained by a fast DFT-based algorithm such as [24].

3.3. Summary of the reconstruction algorithm

Inputs: information signal vector $\mathbf{y}$, sampling sequence Ξ.

1. Initialize parameter boundaries

$$k_{\min} \leqslant k \leqslant k_{\max},$$

$$C_{\min} \leqslant {}^{k}C_i \leqslant C_{\max}, \quad \nu_{\min} \leqslant {}^{k}\nu_i \leqslant \nu_{\max}, \quad \theta_{\min} \leqslant {}^{k}\theta_i \leqslant \theta_{\max}.$$

2. Find parameter vectors

$$\{{}^{k}\hat{\mathbf{C}}, {}^{k}\hat{\boldsymbol{\nu}}, {}^{k}\hat{\boldsymbol{\theta}}\} = \arg \min_{{}^{k}\hat{\mathbf{C}}, {}^{k}\hat{\boldsymbol{\nu}}, {}^{k}\hat{\boldsymbol{\theta}}} \|\hat{\mathbf{y}} - \mathbf{y}\|_2$$

and corresponding objective errors

$${}^{k}O_F = \min_{{}^{k}\hat{\mathbf{C}}, {}^{k}\hat{\boldsymbol{\nu}}, {}^{k}\hat{\boldsymbol{\theta}}} \|\hat{\mathbf{y}} - \mathbf{y}\|_2$$

with

$$\hat{y}_m = \sum_{i=1}^{k} {}^{k}\hat{C}_i \sin(2\pi\, {}^{k}\hat{\nu}_i \xi_m T_s + {}^{k}\hat{\theta}_i), \; m = 1, 2, \ldots, M,$$

for each $k = k_{\min}, k_{\min} + 1, \ldots, k_{\max} - 1, k_{\max}$.

3. Choose optimal parameter vectors according to

$$\hat{K} = \underset{k}{\operatorname{argmin}} ({}^{k}O_F \| {}^{k}\hat{\boldsymbol{\nu}} \|_2).$$

4. Reconstruct the original signal

$$\hat{f}_n = \sum_{i=1}^{\hat{K}} {}^{\hat{K}}\hat{C}_i \sin(2\pi\, {}^{\hat{K}}\hat{\nu}_i n T_s + {}^{\hat{K}}\hat{\theta}_i), \; n = 1, 2, \ldots, N.$$

Outputs:
Parameter vectors ${}^{\hat{k}}\hat{\mathbf{C}}$, ${}^{\hat{k}}\hat{\boldsymbol{\nu}}$, ${}^{\hat{k}}\hat{\boldsymbol{\theta}}$, reconstructed signal $\hat{\mathbf{f}}$.

4. Simulation results

Performance of the proposed reconstruction algorithm was studied using software simulation designed in LabVIEW environment. For all simulations the same test signal was used, generated according to (13) with parameters listed in Table 1. The test signal was generated with sampling period $T_s = 1$, length $N = 1000$ samples and without noise ($q_n = 0$). Sparsity of the test signal is $s = 9$ on (13), resulting in theoretical $M_{\min} = 27$ (3) for SS with DEPE. Of all the $N = 1000$ test signal samples, $M = 50 \cong 5.6s$ were taken according to (14)–(17), providing 1.85 redundancy factor over (3). A new sampling sequence Ξ was generated for each measurement. Experiments have shown that in most cases the reconstruction algorithms either catch on to the input signal (MSE $<$ 0.1) or fail completely (MSE $>$ 1). MSE is dependent to some

Table 1
Test signal parameters.

i	1	2	3
${}^3C_i$	1	2.5	1
${}^3\omega_i$	0.025	0.03	0.035
${}^3\theta_i$	0	0	0

extent on actual distribution of randomly taken samples. For these reasons 100 measurements were performed for each scenario and the MSE was logged. Average mean square error (AMSE) and PSR were calculated, with a threshold of MSE = 0.15 used to discriminate between successful and unsuccessful reconstruction.

The minimization problem (19) was solved using DE with the following constraints: $1 \leqslant k \leqslant 5$, $-3 \leqslant {}^kC_i \leqslant 3$, $0 \leqslant {}^k\theta_i \leqslant \pi$, $0.01 \leqslant {}^k\nu_i \leqslant 0.06$ unless otherwise stated. The reconstruction takes a maximum of a few seconds on an ordinary PC (i7-3770, 8 GB RAM). DE population of 500 and 1000 iterations is sufficient for successful reconstruction while maintaining computational feasibility, as can be seen in Fig. 4. The PSR remains almost 1 with this configuration, even if the input signal is noisy and/or quantized. Number of DE iterations was the only stopping criterium. This arrangement is preferable, as it minimizes the risk of premature termination of the optimization process in a local minimum. An example of input and reconstructed signal waveform is shown in Fig. 5, with estimated signal parameters listed in Table 2.

It is apparent from Fig. 5 that the original and reconstructed signal cannot be easily distinguished by naked eye. With clean test signal the AMSE is 0.013. Frequencies and phases are estimated with precision of 0.01%, amplitudes vary from ideal values by 1.2% mean. Of course, the algorithm will have to deal with nonideal input signal in a practical application. The signal will not be ideally sparse and it will contain inherent and quantization noise. These issues influence the reconstruction error and number of samples required for successful input signal recovery.

A direct compressed sensing reconstruction (DCSR) was implemented and tested for comparison. DCSR reconstruction was performed according to (10) using measurement matrix (17) and a priori defined $\mathbf{\Psi} \in \mathbb{R}^{N\times L}$ basis with elements

$$\psi_{nl} = \begin{cases} \cos(2\pi\nu_{(l-1)}nT_s): \; l = 2k, \quad k \in \mathbb{N} \\ \sin(2\pi\nu_l nT_s) \end{cases} \tag{27}$$

Such base exploits the fact that a sine signal component of any phase can be expressed as a linear combination of sine and cosine of the same frequency. The advantage is lower L than would be needed for a strictly dictionary-like base. The test signal has the sparsity $s = 18$ on (27), resulting in $M_{\min} = 54$. Different s was compensated by taking $M = 100$ samples in performance evaluations of DCSR, thus maintaining $M \cong 5.6s$. Achievable DCSR frequency resolution is determined by the frequency step ν_δ of basis component frequencies

$$\nu_l = \nu_{\min} + l\nu_\delta \tag{28}$$

Unless otherwise stated, the DCSR basis was generated with $0.02 < \nu_l \leqslant 0.045$ and frequency step $\nu_\delta = 5 \times 10^{-5}$, resulting in $L = 1000 = N$. Frequency step this small is required in order to achieve DCSR frequency resolution comparable to DEPE, but results in immense sizes of matrices with wide ν_l frequency spans.

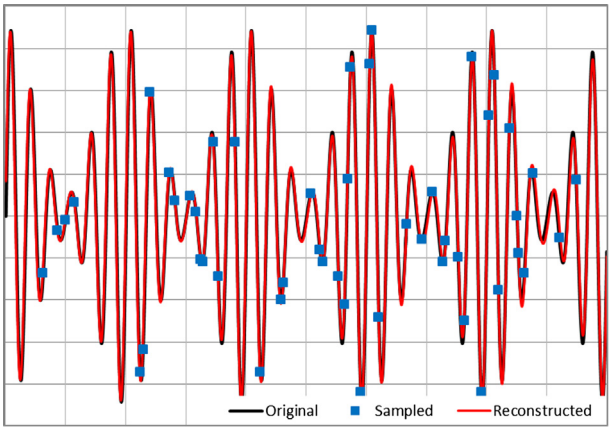

Fig. 5. Clean input signal and reconstructed signal.

Table 2
Estimated clean signal parameters.

i	1	2	3
${}^3C_i$	0.999	2.495	1.002
${}^3\nu_i$	0.0250	0.03	0.03499
${}^3\theta_i$	6.62e-2	1.84e−8	4.22e−3

4.1. A priori knowledge of signal frequency bandwidth

Let the frequency bandwidth investigated by the optimization process be defined with relation to signal bandwidth as

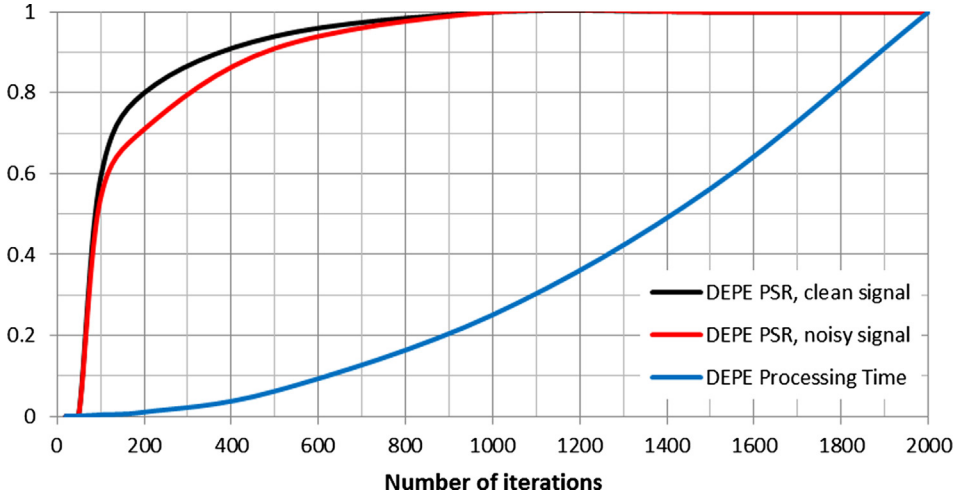

Fig. 4. PSR and relative processing time vs. number of DE iterations.

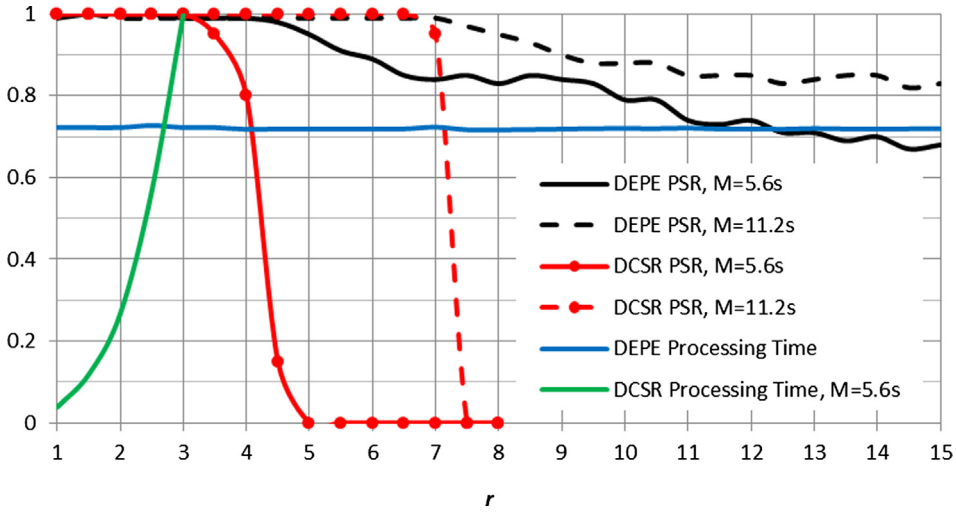

Fig. 6. PSR and relative processing time vs. investigated frequency bandwidth.

$$B(r) = \nu_{\max} - \nu_{\min} = \nu_c \left(\frac{{}^{K}\nu_K}{\nu_c} \right)^r - \nu_c \left(\frac{{}^{K}\nu_1}{\nu_c} \right)^r \tag{29}$$

where ν_c is the signal center frequency

$$\nu_c = \sqrt{{}^{K}\nu_1 \, {}^{K}\nu_K} \tag{30}$$

As it is shown in Fig. 6, the PSR decreases with investigated $B(r)$. The limit until PSR holds is comparable with both DEPE and DCSR, but there is a difference in behavior of the two reconstruction methods above this limit. The DCSR PSR falls almost immediately to zero after (10) is no longer solvable, while there is only a gradual PSR descent with DEPE.

The measured DEPE processing time shown in Fig. 6 is almost constant, since the number of iterations for DEPE was fixed and there were no other stopping criteria. The size of matrices used in DCSR is proportional to $B(r)$, which results in increasing memory usage and processing time. Performance of DCSR was not evaluated above $r = 8$ because of computing hardware limitations. It can be concluded that DCSR is less computationally demanding in scenarios where it is successful, i. e. very small signal parameter variance can be expected and the basis matrix can be constructed accordingly. If the expected variance is greater, DEPE outperforms DCSR while becoming more computationally efficient.

4.2. Number of samples required for successful reconstruction

According to (3), just $M_{\min} = 27$ samples is theoretically enough for successful reconstruction of an ideal signal. The actual successful reconstruction threshold was established by varying the number of samples taken. Resulting AMSE and PSR are shown in Fig. 7.

Simulation results indicate that at least $M = 30$ samples for DEPE and $M = 55$ samples for DCSR must be taken in order to ensure successful input signal recovery, conforming (3). Performance of both algorithms is similar, although smaller $B(r)$ of DCSR was chosen due to results from Section 4.1. It is argued in [25] that according to the discrete sampling theorem, just $M = s$ samples should be enough to restore the original signal regardless of N. The orthogonality of a sine basis conforms this claim, assuming ideal sampling at random time instants. However, with any practical implementation of the *SS*, the time instants at which the samples are taken are not truly random. Input signal is sampled at random integer multiples of an underlying clock, which causes a decrease in incoherence of bases $\mathbf{\Phi}$ and $\mathbf{\Psi}$ [26]. CS thus requires a certain degree of redundancy, expressed by $\log_{10}(N)$ in (3) to compensate for this nonideality. A more general and precise approximation of $M_{\min}$ has been given in [27], but as was pointed out in [28], any analytical derivation of $M_{\min}$ is probabilistic. Choosing M: $s \leqslant M < M_{\min}$ does not mean that the reconstruction is impossible, but rather that there is a high risk of picking particular signal values that result in unsuccessful signal recovery.

4.3. Influence of uncorrelated noise on reconstruction error

With this experiment the input signal was generated as described in Section 4, but with additive Gaussian noise. $M \cong 5.6s$ random samples of this noisy signal were then passed to the reconstruction algorithms. AMSE of both noisy input signal and reconstructed signal were calculated comparing these signals to clean test signal without noise. Results are shown in Fig. 8.

DEPE shows significant robustness against uncorrelated noise. Even very noisy signals can be recovered and the resulting MSE is smaller than MSE of the input signal. All the original signal components are found with the same precision as with clean signal, although noise causes distorting components to appear. Reconstruction partially works even with signals completely drowned in noise. In such cases and with $k_{\min} = 1$ one dominant sine component is correctly found. This is not the case with DCSR, where the PSR rapidly drops by introducing noise. Noise induces an increase in sparsity from $s = 6K$ to virtually $s = N$, which DCSR in conjunction with SS cannot handle. Increasing M on its own does not improve DCSR noise performance unless special measures are taken [29].

An example of input noisy signal with noise standard deviation $\sigma = 1$ (SNR = 6.15 dB) is shown in Fig. 9. Although MSE of the recovered signal is 0.16, it is still a fair approximation of the original clean signal. In Table 3 parameter estimates corresponding to Fig. 9 are shown, where a distorting component appeared at $i = 2$.

4.4. Influence of quantization on reconstruction error

Measurements were performed in the same way as in the previous section. Clean test signal was generated and quantized with a simulated ideal analog to digital converter (ADC) of ± 5 range. The quantizer resolution was varied in the range of 2–20 bits (3–1,048,575 quantization levels). Resulting AMSE of both input quantized signal and reconstructed signal is shown in Fig. 10.

The proposed DEPE algorithm shows superior resistance against quantization noise in comparison with DCSR. There is little influence on the reconstruction error if the signal is quantized with 63 or more quantization levels (corresponding to fully excited 6-bit quantizer). AMSE of the reconstructed signal is lower than the quantized signal MSE for resolutions below 6 bits. Above this threshold, AMSE of the

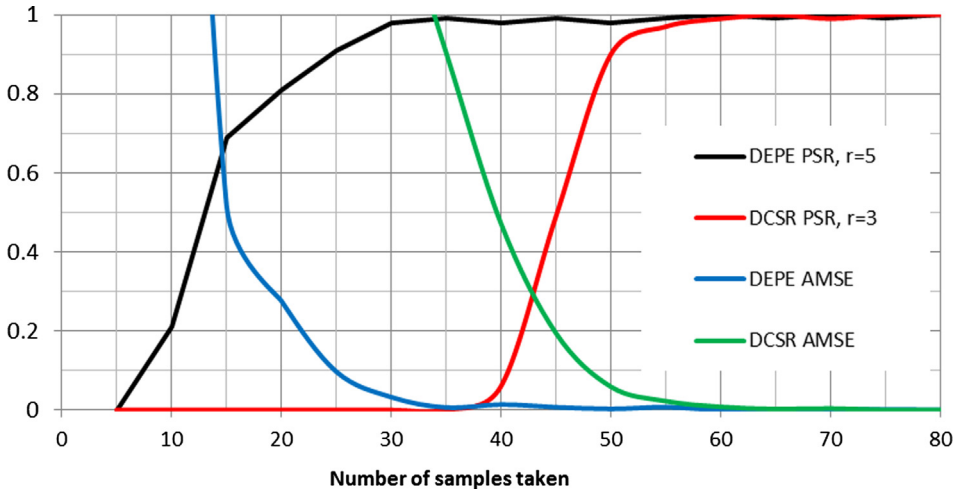

Fig. 7. PSR and reconstruction error vs. number of samples taken.

reconstructed signal is greater, since DEPE never achieves absolute precision with a probability of 1. Signal recovery is possible even with 3-bit quantizer, as is shown in Fig. 11. However, with such low resolutions the reconstruction error depends greatly on actual distribution of samples. Signal parameter estimates corresponding to Fig. 11 are listed in Table 4.Fig. 12.

Quantization noise has similar effect on DEPE as Gaussian noise. With resolutions less than 6 bits the original signal components are usually found, but distorting components also appear.

5. Experimental results

Simulations have shown that the proposed SS framework with DEPE yields satisfactory results. To confirm this, experiments with real hardware were performed. Experimental setup is shown in Fig. 12.

Waveform generator Agilent 33220A was used to generate AM test signals. Actual parameters of these signals were measured using Agilent N9320B spectrum analyser. Test signals were sampled using PC with data acquisition (DAQ) card NI PCIe-6351 and LabVIEW controlling software. With all measurements, the DAQ ADC was set to ± 5 V range and 16bit resolution.

5.1. Stochastic sampling with Nyquist ADC

This experiment was designed to recreate simulation conditions from chap. 4 with real hardware. Input AM signal with $\nu_c = 50$ kHz carrier and $\nu_m = 5$ kHz modulation signal was used, sampled by DAQ card with 1MS/s sampling frequency. The original signal waveform is thus known and can be directly compared to the reconstructed signal. Out of $N = 1000$ Nyquist samples $M = 100$ were randomly taken for reconstruction. The reconstruction constraints were set to $1 \leqslant k \leqslant 5$, $-1\ \text{V} \leqslant {}^{k}C_i \leqslant 1\ \text{V}$, $0 \leqslant {}^{k}\theta_i \leqslant \pi$, $30\ \text{kHz} \leqslant {}^{k}\nu_i \leqslant 80\ \text{kHz}$ $(r \cong 5)$. An

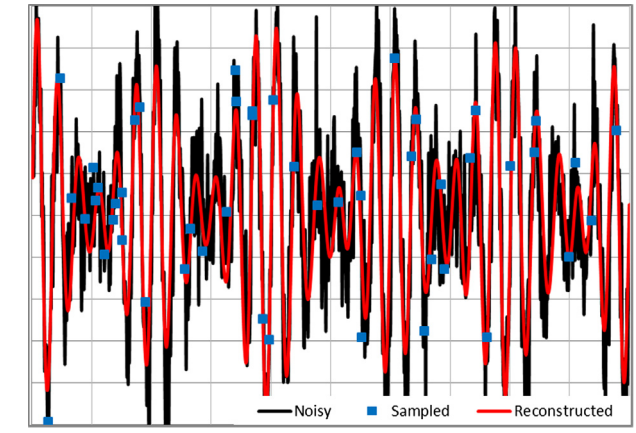

Fig. 9. Noisy input signal and reconstructed signal.

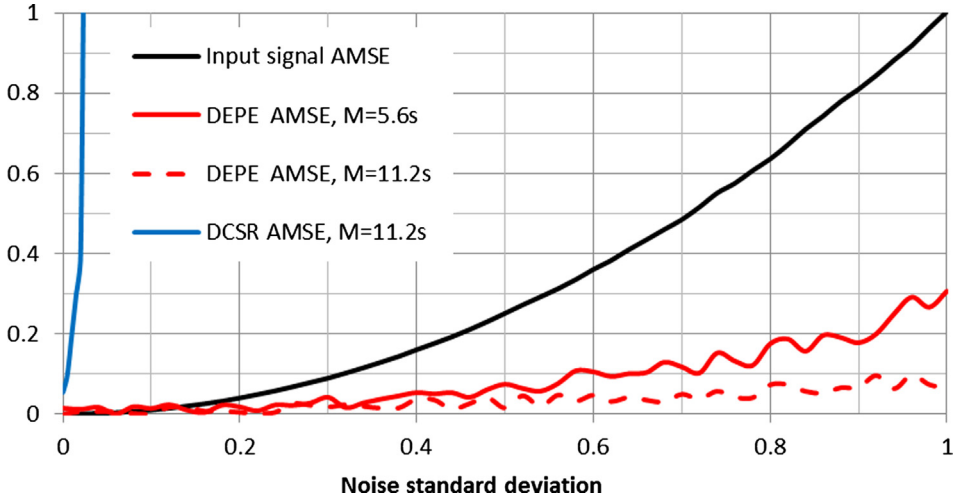

Fig. 8. Influence of uncorrelated noise on reconstruction error.

Table 3
Signal parameters estimated from noisy signal.

i	1	2	3	4
${}^4C_i$	1.038	0.411	2.384	0.948
${}^4\nu_i$	0.0249	0.0277	0.0299	0.0349
${}^4\theta_i$	1.87e−10	0.016	6.25e−11	1.86e−10

example of input and reconstructed signal for $D_m = 50\%$ modulation depth is shown in Fig. 13. Corresponding signal parameters are listed in Tables 5 and 6.

Estimated signal parameters are stable within D_m range of 10–100%. There is a noticeable difference between measured and estimated signal parameters, but estimated values are stable. This can be attributed to signal distortion introduced by analog circuitry of the DAQ card, nonidealities of the ADC and clock setting. Overall, with Nyquist ADC the experimental results confirm the results of simulations.

5.2. Signal recovery with sub-Nyquist ADC

As was mentioned in the introduction, CS allows for lower data transfer rates by not transferring the signal redundancy. This can also be achieved by conventional compression algorithms, but signals need to be acquired with Nyquist sampling rate before compression. Probably the most significant property of CS is therefore its ability to acquire signals with sub-Nyquist rate. Following experiments were performed to demonstrate this fact. Test signals used were AM signals with $f_c = 1$ MHz carrier. The DAQ ADC was set to sampling rate of 480 kS/s (24% of Nyquist rate), which represents the peak sampling frequency limit. An example of respective sampled and reconstructed signal is shown in Fig. 14.

Experiments have shown that in order for DEPE to retain the performance that was demonstrated with simulations, at least 5 periods of the envelope should be randomly sampled. In case of AM signals the envelope period is equal to the period of the modulation signal. The length of processing window T_p during which the samples should be acquired can be determined from the smallest expected proximity of frequency components ν_p as

$$T_p \cong 5/\nu_p \tag{31}$$

With T_p established, the number M of samples to take during this window has to be chosen so that (3) holds. Here the N of (3) is not bound to any physical sampling and can be chosen arbitrarily, but has to comply to the maximum expected signal Nyquist rate $2\nu_{\max}$ with sufficient oversampling ratio for the reconstruction (23):

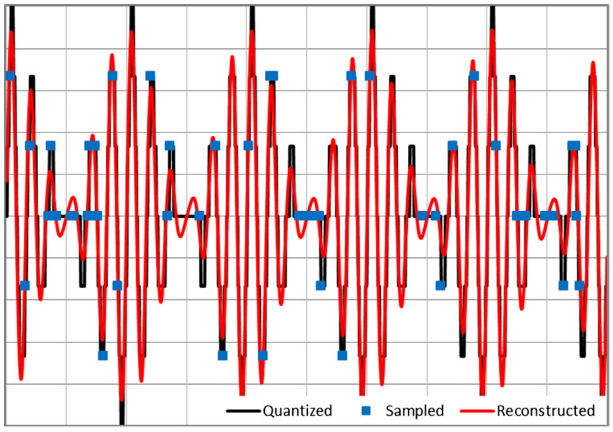

Fig. 11. Quantized input signal and reconstructed signal.

Table 4
Signal parameters estimated from quantized signal.

i	1	2	3
${}^3C_i$	0.878	2.408	1.182
${}^3\nu_i$	0.0250	0.0299	0.0349
${}^3\theta_i$	4.92e-14	1.86e-13	8.89e-12

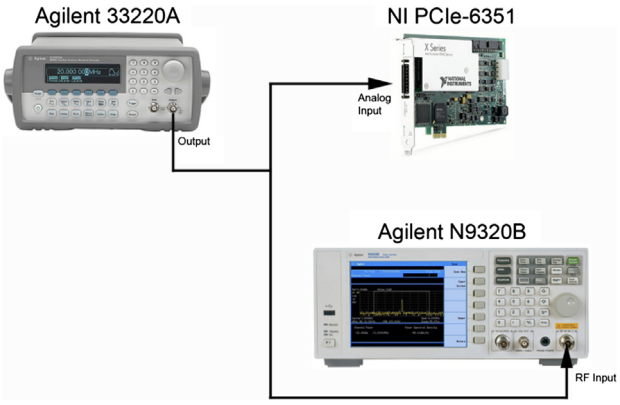

Fig. 12. Experimental setup.

$$N \geqslant 2\nu_{\max} T_p \tag{32}$$

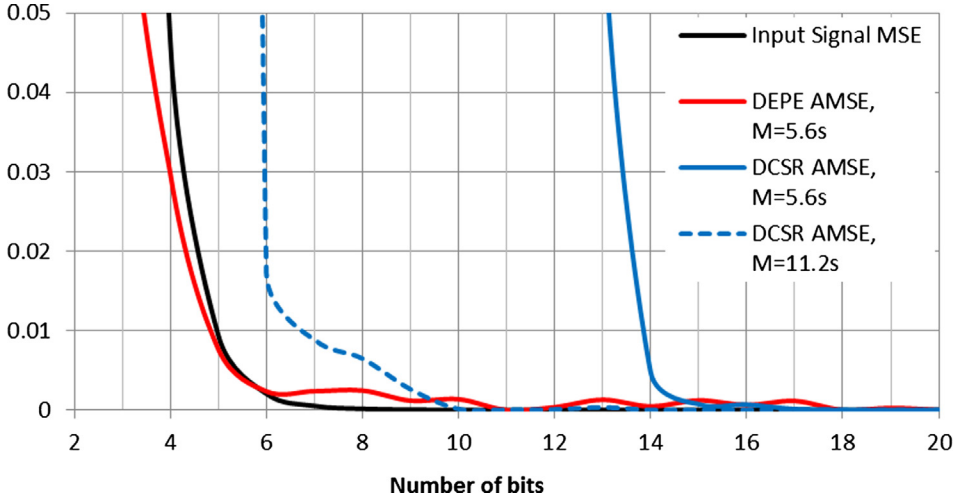

Fig. 10. Influence of quantization noise on reconstruction error.

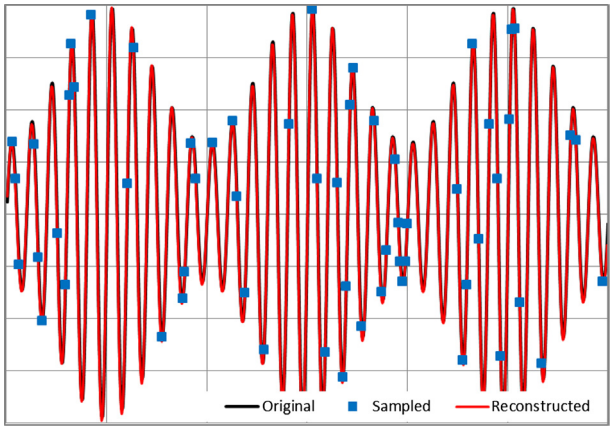

Fig. 13. Acquired input signal and reconstructed signal, $\nu_c = 50$ kHz, $\nu_m = 5$ kHz, $D_m = 50\%$.

Table 5
Measured test signal parameters, $\nu_c = 50$ kHz, $\nu_m = 5$ kHz, $D_m = 50\%$.

i	1	2	3
${}^3C_i$	68.77 mV	280.5 mV	69.81 mV
${}^3\nu_i$	45 kHz	50 kHz	55 kHz

Table 6
Signal parameters estimated from acquired signal, $\nu_c = 50$ kHz, $\nu_m = 5$ kHz, $D_m = 50\%$.

i	1	2	3
${}^3C_i$	−63.92 mV	265.6 mV	63.81 mV
${}^3\nu_i$	44.967 kHz	49.975 kHz	54.979 kHz

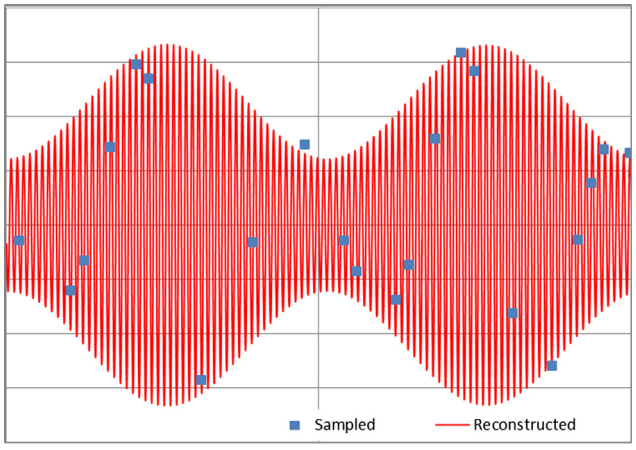

Fig. 14. Acquired samples and reconstructed signal, $\nu_c = 1$ MHz, $\nu_m = 20$ kHz, $D_m = 50\%$.

Table 7
Results for $\nu_c = 1$ MHz, $\nu_m = 1$ kHz, $D_m = 10\%$.

Signal parameter	Measured	Mean estimate	Standard deviation
${}^3C_1$ [mV]	28.56	24.14	1.70
${}^3C_2$ [mV]	566.7	464.79	1.40
${}^3C_3$ [mV]	28.11	21.84	1.72
${}^3\nu_1$ [kHz]	999.007	998.991	0.002,69
${}^3\nu_2$ [kHz]	1000.000	1000.000	0.000,15
${}^3\nu_3$ [kHz]	1000.996	1001.020	0.002,70
Probability of successful reconstruction		87%	

Table 8
Results for $\nu_c = 1$ MHz, $\nu_m = 1$ kHz, $D_m = 50\%$.

Signal parameter	Measured	Mean estimate	Standard deviation
${}^3C_1$ [mV]	141.5	108.6	9.88
${}^3C_2$ [mV]	566.4	-453.6	7.69
${}^3C_3$ [mV]	141.1	121.1	10.03
${}^3\nu_1$ [kHz]	999.007	998.994	0.003,52
${}^3\nu_2$ [kHz]	1000.000	999.986	0.000,97
${}^3\nu_3$ [kHz]	1000.996	1000.980	0.003,38
Probability of successful reconstruction		97%	

Table 9
Results for $\nu_c = 1$ MHz, $\nu_m = 1$ kHz, $D_m = 100\%$.

Signal parameter	Measured	Mean estimate	Standard deviation
${}^3C_1$ [mV]	285.3	-230.8	14.07
${}^3C_2$ [mV]	569.9	449.5	9.31
${}^3C_3$ [mV]	283.5	-221.4	12.81
${}^3\nu_1$ [kHz]	999.007	999.035	0.002,02
${}^3\nu_2$ [kHz]	1000.000	1000.030	0.001,24
${}^3\nu_3$ [kHz]	1000.996	1001.030	0.002,06
Probability of successful reconstruction		97%	

Table 10
Results for $\nu_c = 1$ MHz, $\nu_m = 20$ kHz, $D_m = 10\%$.

Signal parameter	Measured	Mean estimate	Standard deviation
${}^3C_1$ [mV]	27.09	21.41	1.36
${}^3C_2$ [mV]	565.7	-468.6	1.35
${}^3C_3$ [mV]	26.52	21.18	1.14
${}^3\nu_1$ [kHz]	979.913	980.680	0.048,65
${}^3\nu_2$ [kHz]	999.927	1000.010	0.005,20
${}^3\nu_3$ [kHz]	1019.940	1019.340	0.045,73
Probability of successful reconstruction		83%	

Table 11
Results for $\nu_c = 1$ MHz, $\nu_m = 20$ kHz, $D_m = 50\%$.

Signal parameter	Measured	Mean estimate	Standard deviation
${}^3C_1$ [mV]	133.7	111.1	6.49
${}^3C_2$ [mV]	565.6	-460.9	5.67
${}^3C_3$ [mV]	133.5	110.6	5.84
${}^3\nu_1$ [kHz]	979.913	980.177	0.048,18
${}^3\nu_2$ [kHz]	999.927	999.768	0.011,47
${}^3\nu_3$ [kHz]	1019.940	1019.320	0.038,96
Probability of successful reconstruction		98%	

Table 12
Results for $\nu_c = 1$ MHz, $\nu_m = 20$ kHz, $D_m = 100\%$.

Signal parameter	Measured	Mean estimate	Standard deviation
${}^3C_1$ [mV]	267.8	-212.9	14.5
${}^3C_2$ [mV]	565.3	450.1	14.85
${}^3C_3$ [mV]	266.1	-199.6	11.31
${}^3\nu_1$ [kHz]	979.913	980.445	0.045,61
${}^3\nu_2$ [kHz]	999.927	999.742	0.019,68
${}^3\nu_3$ [kHz]	1019.940	1018.980	0.056,54
Probability of successful reconstruction		96%	

Even with long processing window T_p and higher oversampling ratio, condition (3) yields small M and by extension low average sampling rate.

With modulation frequency $\nu_m = 1$ kHz, $M = 200$ samples were

taken within T_p of 5 ms, yielding an average sampling rate of 40 kS/s (2% of Nyquist rate). For test signals with $\nu_m = 20$ kHz, $M = 50$ samples within 250 μs interval were sufficient, resulting in an average sampling rate of 200 kS/s (10% of Nyquist rate). The reconstruction constraints were set to $1 \leqslant k \leqslant 5$, $-1\ \text{V} \leqslant {}^{k}C_i \leqslant 1\ \text{V}$, $0 \leqslant {}^{k}\theta_i \leqslant \pi$, $900\ \text{kHz} \leqslant {}^{k}\nu_i \leqslant 1100\ \text{kHz}$ ($r \cong 5$). 100 measurements were taken for each test signal, and mean and standard deviation of each of the estimated signal parameters were computed.

Results indicate that erroneous measurements occur, which can be discriminated by incorrect number of signal components found or parameter values differing greatly from measured values. Such estimates were excluded from calculation of mean and standard deviation, and were used to assess the probability of successful reconstruction. Results are summarized in Tables 7–12.

There are differences between measured values and mean estimates, which is similar to results from Section 5.1. However, by looking at standard deviations, we can see that the estimation of frequency is precise within a few units to few tens of ppm, depending on input signal. Relative error of mean estimates is greater only by an order of magnitude, meaning it is not caused by the reconstruction algorithm. It can be assumed, that by lowering the sampling frequency below Nyquist rate the influence of aperture uncertainty increases, as is the case with RMPI [9]. Further study of this effect on SS is required.

Estimated amplitudes are stable within range of 6% or less. Mean estimated values equal to cca 80% of measured ones. This is caused by the impulse response of analog circuitry, and could be compensated – input signals are at the top of the frequency range of PCIe-6351 DAQ card.

We emphasize, that we were able to effectively acquire a signal of over 1 MHz bandwidth using an ADC with maximum sampling frequency of only 480 kS/s. Overcoming the Nyquist limit did not require any special hardware. This means that the stochastic sampling framework could be implemented on existing devices as a DSP add-on, thus increasing their input bandwidth.

6. Conclusions

An algorithm for reconstruction of randomly sampled frequency sparse signals was presented. Simulation results indicate that this algorithm is robust against uncorrelated and quantization noise. Original signal recovery is possible even with very noisy signals with SNR $>$ 6 dB. Although this algorithm is computationally demanding, it allows for high compression ratios and precise frequency estimation.

Average sampling rate of random sampler can be as low as 1% of Nyquist rate. At the same time, low resolution ADC may be used. This allows for great reduction of data transfer rate and power consumption with comparison to conventional ADCs.

Random sampler can also overcome the speed limit of Nyquist ADCs. This was demonstrated with a real ADC that acquired samples with peak sampling rate of only 24% of required Nyquist frequency.

CS framework with SS and proposed reconstruction algorithm could be used in applications where frequency sparse signals need to be acquired, analysed, transmitted and stored. Such applications are wireless sensor networks for power grid monitoring, radio frequency coverage mapping or spectrum analysers with sub-Nyquist ADCs.

ACKNOWLEDGMENTS

The work is a part of the project supported by the Cultural and Educational Grant Agency of the Slovak Republic (KEGA No. 015TUKE-4/2016) and the Science Grant Agency of the Slovak Republic (No. 1/0722/18).

References

[1] E. Candes, S. Becker, Compressive sensing: principles and hardware implementations, in: 2013 Proceedings of the ESSCIRC, 2013, pp. 22–23. ISSN 1930-8833.
[2] M. Wakin, S. Becker, E. Nakamura, M. Grant, E. Sovero, D. Ching, J. Yoo, J. Romberg, A. Eami-Neyestanak, E. Candes, A non-uniform sampler for wideband spectrally-sparse environments, IEEE J. Emerg. Sel. Top. Circuits Syst. 2 (3) (2012) 516–529 ISSN 2156-3357.
[3] R. Agarwal, M. Trakimas, S. Sonkusale, Adaptive asynchronous analog to digital conversion for compressed biomedical sensing, in: Biomedical Circuits and Systems Conference, 2009, pp. 69–72. ISBN 978-1-4244-4917-0.
[4] M. Trakimas, S.R. Sonkusale, An adaptive resolution asynchronous ADC architecture for data compression in energy constrained sensing applications, IEEE Trans. Circuits Syst. I: Regular Pap. 58 (5) (2011) 921–934 ISSN 1549-8328.
[5] J.N. Laska, S. Kirolos, M.F. Duarte, T.S. Ragheb, R.G. Baraniuk, Y. Massoud, Theory and implementation of an analog-to-information converter using random demodulation, in: IEEE International Symposium on Circuits and Systems, 2007, pp. 1959–1962. ISBN 1-4244-0920-9.
[6] S. Kirolos, J. Laska, M. Wakin, M. Duarte, D. Baron, T. Ragheb, Y. Massoud, R. Baraniuk, Analog-to-information conversion via random demodulation, in: 2006 IEEE Dallas/CAS Workshop on Design, Applications, Integration and Software, 2006, pp. 71–74. ISBN 1-4244-0670-6.
[7] H. Mamaghanian, N. Khaled, D. Atienza, P. Vandergheinst, Design and exploration of low-power analog to information conversion based on compressed sensing, IEEE J. Emerging Sel. Top. Circuits Syst. 2 (3) (2012) 493–501 ISSN 2156-3357.
[8] P. Daponte, L. De Vito, S. Rapuano, I. Tudosa, Analog-to-information converters in the wideband RF measurement for aerospace applications: current situation and perspectives, IEEE Instrum. Meas. Mag. 20 (1) (2017) 20–28 ISSN 1094-6969.
[9] P. Daponte, L. De Vito, G. Iadarola, S. Rapuano, PRBS non-idealities affecting random demodulation analog-to-information converters, in: 21st IMEKO International Symposium and 19th International Workshop on ADC Modelling and Testing, Budapest, Hungary, 2016, pp. 71–76. ISBN 978-1-5108-3066-0.
[10] P. Daponte, L. De Vito, G. Iadarola, S. Rapuano, Effects of PRBS Jitter on random demodulation analog-to-information converters, in: IEEE Metrology for Aerospace, Florence, Italy, 2016. ISBN 978-1-4673-8292-2.
[11] P. Daponte, L. De Vito, G. Iadarola, M. Iovini, S. Rapuano, Experimental comparison of two mathematical models for Analog-to-Information Converters, in: 21st IMEKO International Symposium and 19th International Workshop on ADC Modelling and Testing, Budapest, Hungary, 2016, pp. 65–70. ISBN 978-1-5108-3066-0.
[12] L. Wu, K. Yu, Y. Hu, Z. Wang, CS-based framework for sparse signal transmission over lossy link, in: IEEE International Conference on Mobile Ad Hoc and Sensor Systems (MASS), Philadelphia, USA, 2014. ISBN 978-1-4799-6036-1.
[13] Z. Slavik, Compressive sensing hardware for analog to information conversion, in: Proceedings of the 8th Karlsruhe Workshop on Software Radios. Karlsruhe: Communications Engineering Lab, 2014, pp. 136–144.
[14] J.C. Whitaker, Oscilloscopes, in: Electronic Systems Maintenance Handbook, second ed., CRC Press, 2002, pp. 2213–2231. ISBN 9780849383540.
[15] Y.C. Eldar, T. Michaeli, Beyond bandlimited sampling, IEEE Signal Process. Mag. 26 (3) (2009) 48–68 ISSN 1053-5888.
[16] Y.C. Eldar, G. Kutyniok, Sensing matrices, in: Compressed Sensing: Theory and Applications, Cambridge University Press, 2012, pp. 15–38. ISBN 978-1-107-00558-7.
[17] E.J. Candes, M.B. Wakin, An introduction to compressive sampling, IEEE Signal Process. Mag. 25 (2) (2008) 21–30 ISSN 1053-5888.
[18] V. Behravan, P.Y. Chiang, R. Farry, N.E. Glover, M. Shoaib, Rate-adaptive compressed-sensing and sparsity variance of biomedical signals, in: 2015 IEEE 12th International Conference on Wearable and Implantable Body Sensor Networks, IEEE, Cambridge, 2015, pp. 1–6. INSPEC 15525171.
[19] M.E. Lopes, Estimating Unknown sparsity in compressed sensing, in: International Conference on Machine Learning (ICML), 2013.
[20] G. Fung, O.L. Mangasarian, Equivalence of minimal ℓ_0 and ℓ_p-norm solutions of linear equalities, inequalities and linear programs for sufficiently small p, Optimization Theory Appl. 151 (1) (2011) 1–10.
[21] E. Candes, J. Romberg, T. Tao, Robust uncertainty principles: exact signal reconstruction from highly incomplete frequency information, IEEE Trans. Inf. Theory 52 (2) (2006) 489–509 ISSN 0018-9448.
[22] D. Agrež, Estimation of signal component from random equivalent and non-coherent sampling measurements, in: ACTA IMEKO, 2011, no. 0, pp. 5–9. ISSN: 2221-870X.
[23] R. Storn, K. Price, Differential evolution, a simple and efficient heuristic for global optimization over continuous spaces, ISSN 1573-2916, J. Global Optimization 11 (1997) 341–359, http://dx.doi.org/10.1023/A:100820282132.
[24] D. Agrež, Periodic signal parameters' estimations from random sampling measurements under non-coherent sampling condition, in: 21st IMEKO International Symposium and 19th International Workshop on ADC Modelling and Testing, Budapest, Hungary, 2016, pp. 190–195. ISBN 978-1-5108-3066-0.
[25] L. Yaroslavsky, Is "Compressed Sensing" compressive? Can it beat the Nyquist sampling approach? in: physics.optics cs.IT math.IT, arXiv:1501.01811v2, 2015.
[26] I. Rish, G.Y. Grabarnik, Mutual coherence, in: Sparse Modeling, CRC Press, 2015, pp. 40–42. ISBN 978-1-4398-2869-4.
[27] H. Boche, R. Calderbank, G. Kutyniok, J. Vybíral, A general framework for compressed sensing based on structured sparsity, in: Compressed Sensing and its Applications, MATHEON Workshop 2013, Springer, 2015, pp. 156–161. ISBN 978-3-319-16041-2.
[28] D. Bellan, S.A. Pignari, Monitoring of electromagnetic environment along high-speed railway lines based on compressive sensing, Progr. Electromag. Res. C. 58 (2015) 183–191 ISSN 1937-8718.
[29] Y.C. Eldar, G. Kutyniok, FRI techniques improving robustness to sampling noise, in: Compressed Sensing: Theory and Applications, Cambridge University Press, 2012, pp. 183–185. ISBN 978-1-107-00558-7.